Monthly Notices
of the
ROYAL ASTRONOMICAL SOCIETY

MNRAS **487,** 3324–3332 (2019)
Advance Access publication 2019 June 3

doi:10.1093/mnras/stz1505

Planet seeding through gas-assisted capture of interstellar objects

Evgeni Grishin ,★ Hagai B. Perets and Yael Avni
Physics Department, Technion - Israel institute of Technology, Haifa 3200002, Israel

Accepted 2019 May 28. Received 2019 May 13; in original form 2019 February 21

ABSTRACT

Planet formation begins with collisional growth of small planetesimals accumulating into larger ones. Such growth occurs while planetesimals are embedded in a gaseous protoplanetary disc. However, small planetesimals experience collisions and gas drag that lead to their destruction on short time-scales, not allowing, or requiring fine-tuned conditions for the efficient growth of ∼metre-sized objects. Here we show that $\sim 10^4$ interstellar objects such as the recently detected 1I/2017-U1 (‘Oumuamua) could have been captured, and become part of the young Solar system, together with up to hundreds of ∼km-sized ones. The capture rates are robust even for conservative assumptions on the protoplanetary disc structure, local stellar environment, and planetesimal interstellar medium density. ‘Seeding’ of such planetesimals then catalyses further planetary growth into planetary embryos, and potentially alleviates the main challenges with the metre-sized growth barrier. The capture model is in synergy with the current leading planet formation theories, providing the missing link to the first planetesimals. Moreover, planetesimal capture provides a far more efficient route for lithopanspermia than previously thought.

Key words: astrobiology – comets: general – minor planets, asteroids: general – minor planets, asteroids: individual: 1I/2017 U1 (‘Oumuamua) – planets and satellites: formation.

1 INTRODUCTION

The early stages of planet formation are thought to occur in gaseous protoplanetary discs (PPD). The primordial PPD consists mostly of gas, and roughly ∼1 per cent of dust (Chiang & Youdin 2010). The small dust grains grow into cm-sized pebbles, which later grow into km-sized planetesimals that later form planets.

While the growth up to cm-sized pebbles and the growth of planetesimals into planets are fairly well understood, the formation of the first planetesimals poses a major challenge. While small grains are tightly coupled to the gas flow and can efficiently grow to mm-cm pebbles, larger ∼metre-sized boulders experience collisional fragmentation and erosion, or interact through bouncing rather than sticking, and are susceptible to strong gas-drag-induced radial drift (Weidenschilling 1977b). Such boulders are therefore rapidly lost, not allowing for planetesimal growth beyond these typical sizes.

Various pathways to overcome the metre-sized barrier problem were suggested (Chiang & Youdin 2010; Blum 2018). These include the gravitational collapse of overdense regions into large planetesimals, where the overdensity of dust and pebbles is catalysed by streaming instabilities (Youdin & Goodman 2005; Johansen et al. 2007). Other channels involve rare cases of successful collisional growth into large planetesimals under favourable conditions in terms of velocity distribution and/or composition (Windmark et al. 2012; Blum 2018; Booth et al. 2018). However, all of these scenarios encounter major challenges and are not robust, as they require highly fine-tuned conditions (see refs. Chiang & Youdin 2010; Blum 2018 for an overview). Once planetesimals reach km size, further growth is achieved by gravitational interactions, and accretion of dust (Xie et al. 2010) or pebbles is efficient in the presence of massive planetary embryos (Ormel & Klahr 2010; Lambrechts & Johansen 2012). One of the main challenges for planet formation is therefore the initial formation of km-sized planetesimals.

The recent flyby of the interstellar object ‘Oumuamua (Meech et al. 2017) suggests that encounters of interstellar planetesimals with different Solar systems are much more common than previously thought (Do, Tucker & Tonry 2018). Such interstellar planetesimals were suggested to be potentially recaptured later on into other Solar systems through purely dynamical processes (Adams & Spergel 2005; Valtonen et al. 2009; Levison et al. 2010; Belbruno et al. 2012; Perets & Kouwenhoven 2012), but they are inefficient and/or occur at late times after planet formation processes take place.

Here we propose that a different efficient *gas-assisted* capture process takes place when a gaseous PPD still exists. Gas–dust/planetesimals interactions are known to play an important role in planet formation and the evolution of bound planetesimals embedded in PPDs (Adachi, Hayashi & Nakazawa 1976; Weidenschilling 1977b; Ćuk & Burns 2004; Perets & Murray-Clay 2011; Fujita et al. 2013; Grishin & Perets 2015). Small grains and pebbles are decelerated by aerodynamic gas drag in the disc. Here we show

★ E-mail: eugeneg@campus.technion.ac.il

that gas-drag-assisted capture of *interstellar* planetesimals capture is no less important.

In this paper, we show that planetesimal capture through this process could play an important role in the initialization and catalysis of efficient planet formation, thereby alleviating the metre-sized barrier problem and providing a robust mechanism for the initial ∼km-sized planetesimal seeds needed for efficient planet formation. Therefore, gas-assisted capture of interstellar planetesimals can potentially resolve some of the main difficulties in our understanding of planet formation through the provision of planetesimal seeds into young PPD.

Our paper is organized as follows: In Section 2 we estimate the encounter rate of interstellar medium (ISM) planetesimals from the mass function of ejected planetesimals (Section 2.1) and the local stellar environment (Section 2.2). In Section 3 we present the analytical planetesimal capture model. We review the PPD structure (Section 3.1), derive the capture condition (Section 3.2) and the capture rates (Section 3.3). We compare our results with Monte Carlo simulations (Section 3.4) and estimate the number of captured objects during the PPD's lifetime (Section 3.5). In Section 4 we discuss the implications and caveats of the model and summarize in Section 5.

2 ENCOUNTER RATE

2.1 Planetesimal mass function

During the planet formation process, a large amount of planetesimals is ejected from a given planet-forming system, and these become unbound interstellar objects (Dones et al. 1999; Melosh 2003). These ejections occur both during the early planet formation phase, or on longer time-scales throughout the stellar and dynamical evolution of the system, long after the PPD dissipates. Adams & Spergel (2005) estimate that for each young star at least $\gtrsim M_\oplus$ of solids are ejected into the ISM with a typical ejection velocity of $\langle v_{\rm eject}\rangle = 6.2 \pm 2.7\,{\rm km\,s^{-1}}$. They consider a mass function of ${\rm d}N_{\rm eject}/{\rm d}m \propto m^{-p}$, where the total number of ejected planetesimals up to mass m is (Adams & Spergel 2005)

$$N_{\rm eject}(m) = \frac{2-p}{p-1}\frac{M_{\rm T}}{m^{p-1}m_{\rm up}^{2-p}} \quad (1)$$

where $M_{\rm T}$ is the total mass, and $m_{\rm up}$ is the upper cut-off of the largest mass possible. Following Adams & Spergel (2005) we adopt $m_{\rm up} = 0.1\,{\rm M_\oplus}$ and $M_{\rm T} = M_\oplus$ (a conservative value).

The power law depends on the details of the formation of the first planetesimals. Adams & Spergel (2005) use a power law with $p = 5/3$, which is also consistent with recent streaming instability (SI) simulations $p = 1.6 \pm 0.1$ (Simon et al. 2017). However, the SI formed planetesimals are too large, ($R \gtrsim 10\,{\rm km}$), and it is more reasonable to consider Dohnanyi-like distributions (Dohnanyi 1969) of collisional cascade, leading to $p = 11/6$ (Raymond et al. 2018a). For $p = 11/6$, the number of ejected planetesimals of mass $>m_1$ is then $N_{\rm eject}(m > m_1) \sim 0.3(m_1/M_\oplus)^{-5/6}$.

Another alternative possibility is that a fraction of interstellar planetesimals was disrupted during ejection (Raymond, Armitage & Veras 2018b found 0.1–1 per cent.) at preferred radius $r_{\rm disr} \approx 100\,{\rm m}$. Given a total mass of $M_{\rm T} \approx 10^{-3}\,{\rm M_\oplus}$, the number of planetesimals of size $r_{\rm disr}$ is $N = M_{\rm T}/(4\pi r_{\rm disr}^3\rho_p/3) \approx 10^{12}$, which is comparable to the number density from the original distribution $N(m_{\rm disr}) \approx 0.3 \times 10^{12}$. Thus, the enhancement is by at most a factor of a few. If there is a distribution of $r_{\rm disr}$, or if $r_{\rm disr}$ is increased, the resulting enhancements will be smaller.

The encounter rate of 'Oumuamua-like objects might be higher. Do et al. (2018) infer a number density of 100 m objects of order $\sim 2 \times 10^{15}\,{\rm pc^{-3}}$, which implies $\sim 10^{16}$ objects are produced per star. Assuming homogeneous objects of the same size, Do et al. (2018) infer that $\sim 50\,{\rm M_\oplus}$ of solids is ejected from each star. Even if planetesimal mass function is ignored, this scenario is implausible since the solid disc reservoir per star is insufficient and alternative scenarios are suggested. In what follows we compare our nominal rate with enhanced rates based on the estimate of Do et al. (2018). We enhance the total mass of ejected planetesimals to $M_{\rm T} = 50\,{\rm M_\oplus}$, but keep the planetesimal mass function.

2.2 Encounter rates at different environments

The number of planetesimals entering the disc region is therefore $N_{\rm enter} \approx n_{\rm ISM}\sigma_{\rm env}\langle v\rangle\tau_{\rm env}$, where $n_{\rm ISM} = n_\star N_{\rm eject}$ is the number density of interstellar planetesimals, $n_\star$ is the number density of stars, $\sigma_{\rm env} = \pi b_{\rm max}^2$ is the cross-section, with a maximal impact parameter $b_{\rm max}$, above which no significant encounter occurs, $\langle v\rangle = \sqrt{8/\pi}\sigma$ is the mean velocity where σ is the velocity dispersion of the environment, and $\tau_{\rm env}$ is a typical time-scale during which encounters with the disc can occur.

One may consider two types of environments; (1) A cluster-/stellar-association environment in which a group of stars is bound together and their relative velocities are low; and (2) a field environment where stars and/or interstellar planetesimals are unrelated to each other and the relative velocities between them are high. For the cluster environment we consider a stellar density of $n_\star^c \sim 750/\pi N_\star^{1/2}\,{\rm pc^{-3}}$, where $N_\star = 100$–1000. In this case, the velocity is dominated by the dispersion velocity of ejected planetesimals $\sigma = 6.2 \pm 2.7\,{\rm km\,s^{-1}}$ (Adams & Spergel 2005). In the field, the velocity is dominated by the (observed) stellar velocity dispersion $\sigma \sim 30\,{\rm km\,s^{-1}}$, and the stellar density is $n_\star^f \sim 0.1\,{\rm pc^{-3}}$. Young systems are likely to form in the central parts of the Galactic disc (De Simone, Wu & Tremaine 2004). The velocity dispersion of young stars and stars residing in the central part of the disc is therefore typically lower than assumed here (i.e. $\sim 20\,{\rm km\,s^{-1}}$), and therefore our fiducial choice is likely to be conservative. Moreover, additional environments can be considered, such as globular clusters, and moving stellar groups (De Simone et al. 2004) that have larger number density or small velocity dispersion, respectively.

For the cluster, $\tau_{\rm env} = r/\sigma \sim 0.3\,{\rm Myr}$ is the cluster crossing time. In the field, the typical time is dominated by the disc lifetime $\tau_{\rm env} = t_{\rm disc} = 3\,{\rm Myr}$. In the case of a young cluster environment the timing of material ejection is important. In particular, if ejections take place at times much longer than the lifetime of PPDs they will not contribute to the reservoir of interstellar planetesimals available for capture. However, models suggest the actual time-scale for material ejection is comparable to that of the gaseous disc lifetime (Morbidelli 2018).

Using the aforementioned relations, the number of planetesimals that enter the PPD as a function of their size is given by

$$N_{\rm enter}(R) = N_{\rm eject}(R) n_\star b_{\rm max}^2 \sqrt{8\pi}\sigma\tau_{\rm env}. \quad (2)$$

For field (cluster) environments the typical numbers are $n_\star = 0.1$ $(7.5)\,{\rm pc^{-3}}$, $b_{\rm max} = 50$ $(130)\,{\rm au}$, $\sigma = 30$ $(6.2)\,{\rm km\,s^{-1}}$, $\tau_{\rm env} = 3$ $(0.3)\,{\rm Myr}$, leading to $N_{\rm enter}(R > 1\,{\rm km}) \approx 10^4$ (1.1×10^5) $(R/{\rm km})^{-5/2}$. This is likely a lower limit, since the inferred encounter rate of 'Oumuamua-like objects (with effective diameter of ∼100 m), given its recent detection, is at least ∼50 times higher than the above estimated rate for 100 m-sized bodies entering the Solar system in today's field environment (Do et al. 2018).

3 CAPTURE RATES

3.1 Protoplanetary disc structure

The radial and vertical structure of the PPD can be modelled from the Chiang–Goldreich simple flared disc model (Chiang & Goldreich 1997). The radial gas surface density is $\Sigma_g = \Sigma_{g,0}(a/\mathrm{au})^{-\beta}$, where $\Sigma_{g,0} = 2 \times 10^3 \mathrm{g\ cm^{-2}}$. The normalization Σ_0 and scaling $\beta = 3/2$ corresponds to the Minimal Mass Solar Nebula (MMSN) profile (Weidenschilling 1977a; Hayashi 1981). Larger normalizations and various power laws ($\beta \sim 0.5$–2.2) have been invoked in order to explain the formation of super-Earth planets, though there is a large spread and uncertainty in the observed systems (Chiang & Laughlin 2013; Raymond & Cossou 2014).

The vertical structure is governed by hydrostatic equilibrium, which leads to a Gaussian profile, where in cylindrical coordinates $\rho_g(r, z) = \rho_g(r, 0)\exp(-z^2/2h^2)$, where $h = c_s/\Omega$ is the disc scale height, c_s and Ω is the sound speed and the Keplerian frequency, respectively (Perets & Murray-Clay 2011; Grishin & Perets 2015). The surface density is then $\Sigma_g(r) = \int \rho_g(r, z)\mathrm{d}z = \sqrt{2\pi}h\rho(r, 0)$.

3.2 Capture condition

Consider an interstellar object coming from infinity with velocity $\boldsymbol{v}_\infty$, going through a gaseous PPD around a star of mass $M_\star$. For a spherical body with density $\rho_p = 1\ \mathrm{g\ cm^{-3}}$, radius R_p, and relative velocity $\boldsymbol{v}_{rel}$ which crosses a region of the disc with density ρ_g, the aerodynamic gas drag force is

$$\boldsymbol{F}_D = -\frac{1}{2}C_D \pi R_p^2 \rho_g v_{rel}^2 \hat{\boldsymbol{v}}_{rel}, \tag{3}$$

where $C_D(\mathcal{R}e)$ is the drag coefficient, which depends on the Reynolds number $\mathcal{R}e = R_p v_{rel}/\nu_m$, where $\nu_m = (1/2)\bar{v}_{th}\lambda$ is the molecular viscosity of the gas, $\bar{v}_{th}$ is the thermal velocity, and λ is the mean free path of gas–gas collisions.

Large planetesimals are in the ram pressure regime with constant coefficient $C_D = 0.44$. Small dust grains are in the Epstein regime, with $C_D \propto R_p^{-1}$. The transition to Stokes regime occurs at $R_p = 9\lambda/4$. In the Stokes regime, $C_D \propto R_p^{-3/5}$. We follow the prescription of Perets & Murray-Clay (2011) for the Reynolds number and drag laws.

For a planetesimal that crosses the disc face on at radial location $\bar{a}$, the amount of energy loss during the interaction with the disc is the total work applied on the planetesimal

$$\Delta E = \int \boldsymbol{F}_D \cdot \boldsymbol{v}_{rel}\mathrm{d}t = -\frac{\pi C_D R_p^2 \rho_0}{2}\int_{-\infty}^{\infty} \exp\left(-\frac{v_{rel}^2 t^2}{2h^2}\right) v_{rel}^3 \mathrm{d}t$$

$$\approx -\frac{\pi C_D}{2} R_p^2 \Sigma_g v_{rel}^2, \tag{4}$$

where $\rho_0 = \rho_g(\bar{a}, z = 0)$ is the density at the mid-plane, and we assume that the relative velocity $\boldsymbol{v}_{rel} = \boldsymbol{v}_\infty + \boldsymbol{v}_{esc}(\bar{a})$ is constant throughout the passage, where $v_{esc} = \sqrt{2GM_\star/\bar{a}}$ is the escape velocity.

There are two regimes: Either $v_\infty \gg v_{esc}$, the geometrical regime, or $v_\infty \ll v_{esc}$, gravitational focusing regime, letting $v_{rel}^2 \approx v_\infty^2 + v_{esc}^2$ takes both options into account.

The body is captured if it has dissipated more energy than its initial energy $E_{in} = m_p v_\infty^2/2$, or $|\Delta E| > E_{in}$. In terms of the body's size, the capture condition is

$$R_p \lesssim \frac{3}{4}\frac{C_D \Sigma_g}{\rho_p}(1 + \Theta_s), \tag{5}$$

where $\Theta_s \equiv v_{esc}^2/v_\infty^2$ is the gravitational focusing Safronov number. For $\Theta_s \gg 1$ gravitational focusing is important, while for $\Theta_s \ll 1$ the scattering is mostly in the geometric collision regime. Intuitively, in the geometric regime, capture requires a velocity change of order of the incident velocity $\delta v \sim v_\infty$, thus corresponds to a requirement that the disc surface density exceeds a fixed fraction of the planetesimal mass per unit area.

Fig. 1 shows an example of a typical trajectory and evolution of interstellar planetesimals as they encounter the disc, dissipate their energy, and become embedded in the disc. In the following we use a detailed analysis to provide a quantitative study of the capture rate of such planetesimals.

3.3 Capture rates

In order to evaluate the fractions and total number of planetesimals captured through this process, we need to consider the properties of the orbits and the PPD, as well as properties of the environment.

For the encounter properties, we consider the distributions of the velocity, impact parameters, and relative impact angles to the disc, as well as the size distribution of the incoming planetesimals. We assume that interstellar objects have a Maxwellian velocity distribution (similar to their progenitor stellar hosts)

$$f_V(v_\infty, \sigma) = \sqrt{\frac{2}{\pi}}\frac{v^2}{\sigma^3}\exp\left(-\frac{v_\infty^2}{2\sigma^2}\right);\ v \in [0, \infty), \tag{6}$$

where σ is the velocity dispersion. Faster planetesimals collide more frequently so the distribution of rate of collisions per unit time is further weighted by an additional factor of v_∞. The distribution of impact parameters follows a simple geometric cross-section, i.e. a uniform distribution of the impact parameter $B^2 \sim U[0, b_{max}^2]$ (the trajectory can later change due to gravitational focusing, which we account for when relevant), where b_{max} is the maximal impact parameter for an effective close encounter. Both of these depend on the stellar environment.

3.3.1 *Geometric regime*

In this case $\Theta_s \ll 1$ (negligible gravitational focusing), i.e. the trajectory of an incoming interstellar planetesimals follows a straight line before encountering the disc, and is negligibly affected by the gravitational pull from the host star. The capture criterion is then

$$\frac{3C_D\Sigma_g}{4\rho_p R_p} < 1\,. \tag{7}$$

taking a density profile $\Sigma_g = \Sigma_{g,0}(a/\mathrm{au})^{-\beta}$ we get

$$\left(\frac{a}{\mathrm{au}}\right)^\beta < \frac{3C_D\Sigma_{g,0}}{4\rho_p R_p}\,. \tag{8}$$

For geometric scattering, the closest approach is $q \approx b$, so the criterion is

$$b_c(R_p) < \left(\frac{3C_D\Sigma_{g,0}}{4\rho_p R_p}\right)^{1/\beta}\mathrm{au}, \tag{9}$$

or with the dimensionless parameter $x = b_c/b_{max}$, the capture probability is

$$f_c(R_p) = \left(\frac{b_c}{b_{max}}\right)^2 = \left(\frac{3C_D\Sigma_{g,0}}{4\rho_p R_p}\right)^{2/\beta}\left(\frac{\mathrm{au}}{b_{max}}\right)^2$$

$$= 0.16\left(\frac{C_D}{25}\right)^{4/3}\left(\frac{b_{max}}{130\,\mathrm{au}}\right)^{-2}\left(\frac{R_p}{2\,\mathrm{m}}\right)^{-4/3}, \tag{10}$$

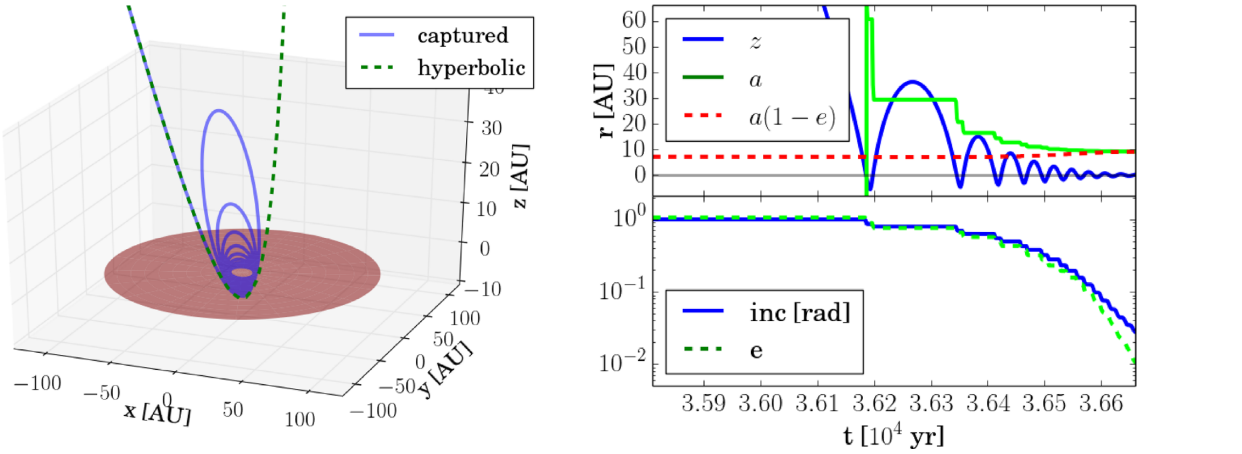

Figure 1. Flyby and capture orbits of interstellar planetesimals. Left: The 3D trajectories of initially hyperbolic, interstellar planetesimals. The dashed green line represents a hyperbolic (non-capture) encounter, similar case of 'Oumuamua, for planetesimals of size $R_p = 10^4$ m. The blue line corresponds to a smaller planetesimal ($R_p = 10$ m) which efficiently dissipates its energy through gas drag, decelerates and becomes embedded in the disc (red circle). The initial orbital elements are the same. Right: Time evolution of the orbital elements of the captured orbit. Top panel shows the evolution of the height z above the PPD, the semimajor axis a and the pericentre approach $a(1-e)$. The bottom panel shows the evolution of the inclination and the eccentricity e.

where we used $\beta = 3/2$ and the disc normalization of Section 2.1. The geometric regime is independent of the initial velocity and the PPD profile. The geometric regime is valid mostly for small grains and pebbles, and thus neglecting gravitational focusing underpredicts the capture probability of large $\gtrsim$100 m planetesimals.

3.3.2 *Gravitational focusing regime*

In the gravitational focusing regime, ($\Theta_s \gg 1$; which corresponds to small impact parameters and/or low velocities), the capture condition is

$$\left(\frac{a}{\mathrm{au}}\right)^{\beta} v_\infty^2 < \frac{3C_D\Sigma_{g,0}}{2\rho_p R_p}\frac{GM}{a}, \tag{11}$$

which depends both on the velocity and the impact parameter. In order to proceed, we use the parabolic approximation to find the closest approach $a = q$,

$$q = \frac{GM}{v_\infty^2}\left[\sqrt{1+\frac{b^2v_\infty^4}{G^2M^2}} - 1\right] \approx \frac{b^2v_\infty^2}{2GM} \tag{12}$$

so the capture condition is

$$b^{2(1+\beta)} \le 2^\beta \frac{3C_D\Sigma_{g,0}}{\rho_p R_p}\left(\frac{GM}{v_\infty^2\,\mathrm{au}}\right)^{2+\beta}\mathrm{au}^{2(1+\beta)} \equiv b_c^{2(1+\beta)}. \tag{13}$$

The velocity dependent capture probability is

$$P_c(R_p|v_\infty) = \int_0^{b_c(v_\infty)} f_B(b)\mathrm{d}b = \left(\frac{b_c(v_\infty)}{b_{\max}}\right)^2, \tag{14}$$

where $b_c(v_\infty)$ is given by equality in equation (11). Now we want to look at the different rates of arrival: faster planetesimals have higher encounter rates than slower one. The integrals that involve the probability have an additional v factor, e.g. $P \propto \int v f_V(v)\mathrm{d}v$. Namely, the weighted capture probability for a given time is

$$f_c(R_p) = \frac{N_{\mathrm{captured}}(R_p)}{N_{\mathrm{enter}}(R_p)} = \frac{\int N_{\mathrm{enter}}(v, R_p, b_{\max}) f_V(v_\infty) P_c(R_p|v_\infty)\mathrm{d}v_\infty}{\int N_{\mathrm{enter}}(v, R_p, b_{\max}) f_V(v_\infty)\mathrm{d}v_\infty}. \tag{15}$$

Since $N_{\mathrm{enter}}(R_p) \propto v_\infty$ we have

$$f_c(R_p) = \frac{1}{\langle v_\infty\rangle_{f_V}}\int v_\infty f_V(v_\infty) P_c(R_p|v_\infty)\mathrm{d}v_\infty = \iint_{D_c}\frac{2b}{b_{\max}^2}\frac{v^3}{2\sigma^4}\mathrm{e}^{-v^2/2\sigma^2}\mathrm{d}b\mathrm{d}v, \tag{16}$$

where $\langle v_\infty\rangle_{f_V} = \sqrt{8/\pi}\sigma$ is the mean thermal speed. The integration is on the fractional domain D_c of parameters that result in capture.

The latter is equivalent to drawing the velocity from a $\chi(4)$ distribution:

$$\tilde{f}_V(v) = \frac{1}{2}\frac{v^3}{\sigma^4}\exp\left(-\frac{v^2}{2\sigma^2}\right). \tag{17}$$

The capture probability is encapsulated in the new random variable $x \equiv (b/b_{\max})^\alpha (v_\infty/\sigma)^2$, where $\alpha = 2(1+\beta)/(2+\beta)$. We show in Appendix A that the distribution function for x can be expressed in terms of incomplete Gamma functions,

$$f_X(x) = 2^{-(2+\beta)/(1+\beta)}\frac{2+\beta}{1+\beta}\Gamma\left(\frac{\beta}{1+\beta}, \frac{x}{2}\right)x^{1/(1+\beta)}. \tag{18}$$

For the special case of $\beta = 3/2$, $f_X(x) \propto x^{2/5}\Gamma\left(\frac{3}{5}, \frac{x}{2}\right)$. The weighted capture probability is

$$f_c(R_p) = \int_0^{x_c(R_p)} f_X(x)\mathrm{d}x$$

$$x_c = 2^{\beta/(2+\beta)}\left(\frac{3C_D\Sigma_0}{\rho_p R_p}\right)^{1/(2+\beta)}\left(\frac{GM}{\sigma^2\mathrm{au}}\right)\left(\frac{b_{\max}}{\mathrm{au}}\right)^{-\alpha(\beta)}. \tag{19}$$

Since the gravitational focusing regime is relevant for large planetesimals, it requires close approach, which is possible only with either small velocity or impact parameter. In either case, $x_c \ll 1$, and the (weighted) probability (equation 3.3.2) can be expanded into leading terms,

$$f_c(x_c) = \left(\frac{x_c}{2}\right)^{(2+\beta)/(1+\beta)}\Gamma\left(\frac{\beta}{1+\beta}\right) + \mathcal{O}(x_c^2). \tag{20}$$

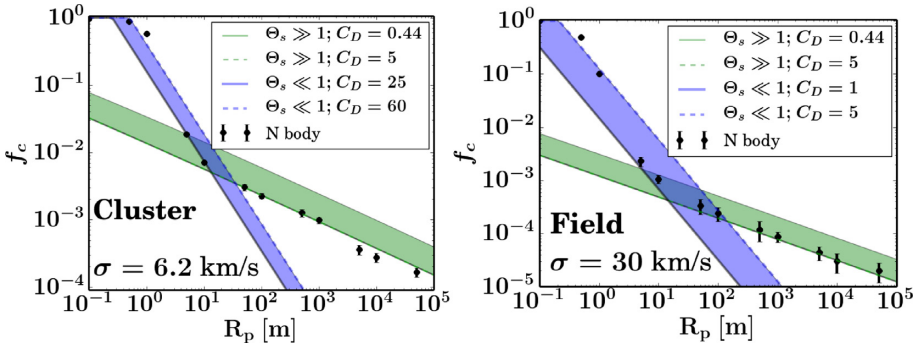

Figure 2. Fractions of captured planetesimals as a function of their size. Blue area is the estimated probability in the geometric scattering regime, green area is the estimated probability in the gravitational focusing regime. Black dots are result of a numerical simulation. The error bars are estimated from shot noise of the captured orbits. Choices of drag coefficients are discussed in the Methods. Generally, planetesimals above $R_p \gtrsim 100$ m follow the gravitational focusing prediction $f_c \propto R_p^{-2/5}$. The transition to geometric scattering regime is near ∼10 m for both environments ∼100 m.

For the special case $\beta = 3/2$ we have

$$f_c(R_p) = \frac{\Gamma\left(\frac{3}{5}\right)}{2^{7/5}} x_c^{7/5} + \mathcal{O}(x_c^2)$$

$$\approx 0.86 \left(\frac{3C_D\Sigma_0}{\rho_p R_p}\right)^{2/5} \left(\frac{GM}{\sigma^2 \mathrm{au}}\right)^{7/5} \left(\frac{b_{max}}{\mathrm{au}}\right)^{-2}. \quad (21)$$

Note that in either regime of the capture fraction (equation 3.3.1 and 3.3.2) it is proportional to $\propto b_{max}^{-2}$, which cancels out with the $\propto b_{max}^2$ from the encounter rate. Thus, the total number of captured planetesimals $N_{enter} \cdot f_c$ is independent of b_{max}, hence the choice of b_{max} is rather arbitrary, as expected. Multiplying by $n_{ISM}(\sqrt{8/\pi}\sigma)\pi b_{max}^2$ yields the total number of captures:

$$N(R_p) \approx 4.29 \left(\frac{3C_D\Sigma_0}{\rho_p R_p}\right)^{2/5} \left(\frac{GM}{\sigma^2 \mathrm{au}}\right)^{7/5} n_{ISM}\sigma\tau_{env}\mathrm{au}^2, \quad (22)$$

and it is independent of b_{max}, as expected.

Fig. 2 shows the comparison between the analytic estimates and the simulations. Small pebbles, up to ∼1 m, are the most susceptible to gas drag, and are efficiently captured. These can be captured even at the lower density regimes of the disc at large separations. Larger planetesimals require progressively close pericentre approach of their trajectory, near the high-density inner regions of the disc. Therefore, large planetesimals are in the gravitational focusing regime, where the gas drag is ram pressure dominated and the drag coefficient has a constant value $C_D = 0.44$. For geometric scattering we expect to be somewhere near the Epstein–Stokes transition, i.e. near $C_D = 24$.

Fig. 2 shows good converge of the analytical models, both in the power-law scaling and in the gas drag regime. Planetesimals in the field have much higher velocities and Reynolds numbers, hence they are rarely in the Epstein regime and have smaller drag coefficients.

3.4 Numerical modelling and comparison

In order to better verify the analytical estimates, we run *N*-body simulations that include gravity and a prescription for gas drag (equation 3), based on fourth-order Hermite integrator (Hut, Makino & McMillan 1995). We truncate the disc density at $r_{disc} = 250$ au. The aspect ratio is $h/r = 0.022(r/\mathrm{au})^{2/7}$. The velocity of the gas is slightly sub-Keplerian due to pressure gradients, namely $v_{gas} = \eta v_{Kep}$, with $\eta = (1 - (3/2 + \beta + 3/14)(h/r)^2)^{1/2}$ (see Grishin & Perets 2015, 2016 for more details). The relative velocity is $\boldsymbol{v}_{rel} = \boldsymbol{v}_p - \boldsymbol{v}_{gas}$, where $\boldsymbol{v}_p$ is given in Cartesian coordinates after rotation of the hyperbolic orbit to the disc's reference plane. We initialize the planetesimal to start from $r_0 = 20\,000$ au with orbital parameters and disc inclination drawn from distributions described in the main text. We stop the simulation if the distance from the sun exceeds 50 000 au and negative energy and conclude the orbit is unbound. For bound orbits we stop if either the distance is $r < 0.02$ au or the orbital eccentricity is $e < 0.1$.

For each planetesimal size we run $10^4 - 3 \times 10^5$ numerical integrations with b and v_∞ distributed from uniform in b^2 and $\chi(4)$ distributions, respectively. The relative angles between the planetesimal trajectories and the PPD were drawn from an isotropic distribution (uniform in the argument of pericentre and the longitude of ascending node angles, and uniform in the cosine of the inclination angle).

3.5 Total number of captured planetesimals and radial distribution

Using the size-dependent capture probability, we obtain the total number of captured planetesimals of a given size.

The left-hand panel of Fig. 3 shows the expected size-dependent number of captured planetesimals for a collisional planetesimal mass function with $p = 11/6$. Many small pebbles and planetesimals up to $\lesssim$100 m are captured, which could lead to efficient seeding and subsequent planet formation. At least one planetesimal as large as ∼6 km (∼1 km) is captured in a cluster (field) environment. The inferred rate, based on 'Oumuamua passage, is enhanced by ∼50 times. The latter would then result in the capture of even ∼23 km (∼4 km) for a cluster (field) environment. The right-hand panel of Fig. 3 shows the number of captured planetesimals from SI mass function, $p = 5/3$. In this case, there are less planetesimals to begin with, therefore the overall numbers are lower, although still significant.

Fig. 4 shows the empirical cumulative radial distribution of captured planetesimals for different size ranges. As mentioned above, disc dissipation can be efficient for small planetesimals even at the disc outskirts where the gas densities are low. The capture of larger planetesimals, however, requires higher gas densities. Therefore the larger the planetesimals, the more centrally concentrated is their radial distribution.

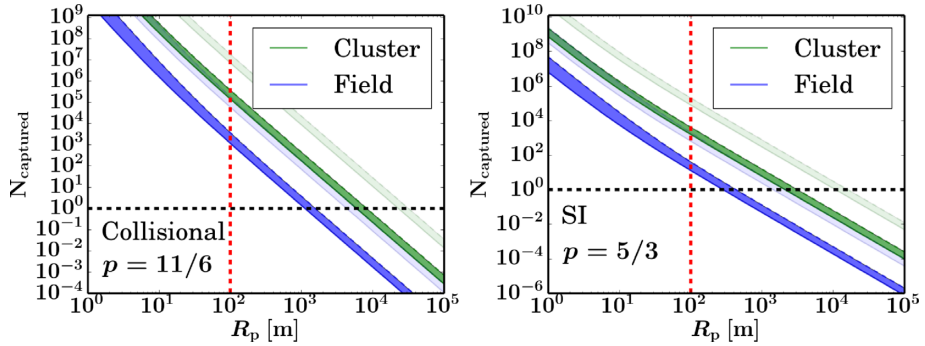

Figure 3. The number of captured planetesimals during a typical lifetime τ_{env}, given the theoretically estimated rates. The left-hand and right-hand panels represent collisional (Dohnanyi) and SI induced mass functions, respectively. Green area corresponds to the rates for the cluster, while blue area corresponds to the rates for the field. The boundaries are determined by different drag coefficients, similar to Fig. 2. Red vertical line stands for the effective radius of 'Oumuamua, ∼100 m. The observed rate, based on 'Oumuamua passage, are enhanced by ∼50 times. The enhanced rates represented by the transparent green and blue areas for the cluster and the field, respectively.

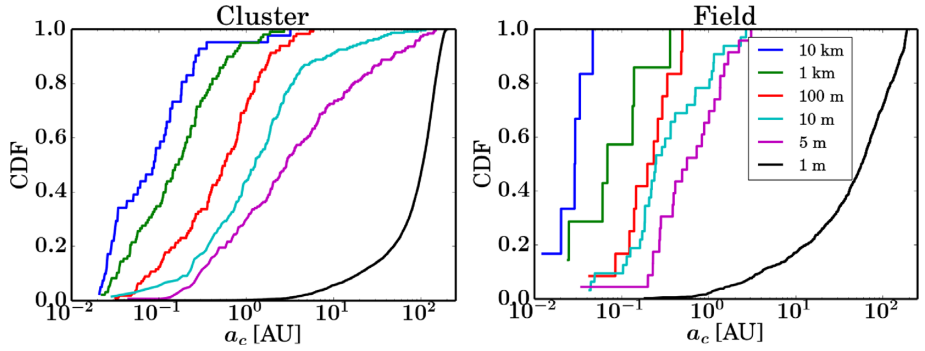

Figure 4. The size-dependent cumulative radial distribution of captured planetesimals. Several planetesimal sizes are shown; $R_p = 10^4,\ 10^3\ ,100,\ 10\ ,5\ ,1$ m (blue, green, red, cyan, purple, and black respectively), for the cluster (left) and the field (right). Once captured, the circularization time-scale is much shorter than radial drift time-scales (see Fig. 1b and Adachi et al. 1976), thus the final semimajor axis is close to the first pericentre approach.

4 DISCUSSION

4.1 The metre size barrier and the first planetesimals

The gas-assisted capture mechanism can seed a few up to thousands of ∼km-sized planetesimals in the disc. Such relatively small number of seeds can then rapidly grow to 100 km size on short time-scales before collisional erosion starts (although for a fraction of systems with extremely strong turbulence planetesimals may not grow by dust accretion, Xie et al. 2010). We therefore expect the effective initial distribution of cores and asteroids to be at large radii, somewhat similar to that expected from the SI models and consistent with suggestions and observations that asteroids were born big and that the asteroids were formed from a small number of asteroid families (Morbidelli et al. 2009; Dermott et al. 2018). A fraction of these grown planetesimals later ejected from the systems, and further replenish the population of interstellar planetesimals. These, in turn, can be recaptured by other systems and further catalyse planet formation, and so on, i.e. leading to a chain reaction – like exponential planet-seeding process.

One may still question how did large planetesimals and later planets formed in the first system that initialized the seeding. Formation of km-sized planetesimals is a long-standing problem in planet formation theories (Chiang & Youdin 2010; Blum 2018). The disc capture scenario cannot account for this initial formation, however, it can alleviate the problem, by allowing for the first formation of such planetesimals to be a rare event, and even under fine-tuned condition.

4.2 Initial population and propagation

We have assumed that every star has contributed to the ISM planetesimal population. Here we present an order of magnitude estimate on the fraction of stars required to initially produce ISM planetesimals and find that even one star per cluster could be sufficient. More accurate estimations that verify or negate our results and assumptions should be developed in the future.

Assuming that only a fraction $f_\star$ of stars forms planetesimals, the spatial distribution of planetesimals is uniform after a mixing time $\tau_\star \sim l_\star/\sigma \propto (n_\star f_\star)^{-1/3}\sigma^{-1}$, where $l_\star$ is the average distance between stars that contribute planetesimals. Remarkably, the combination $n_\star^{1/3}\sigma$ has roughly the same value for both cluster and field environments, therefore the mixing time $\tau_\star$ depends only on the fraction $f_\star$, and not on the environment. As long as the mixing time is less than the disc lifetime, we evaluate the capture rate as before, only with the number density of ejected planetesimals multiplied by $f_\star$ that account for the efficiency of planetesimal formation per star.

Most stars are thought to form in stellar associations and clusters. Even if only one star in an $N_\star \sim 1000$ ($f_\star = 10^{-3}$) cluster contributes planetesimals, the cluster mixing time is comparable to the crossing time and much less than the disc lifetime $\tau_{env} \sim 0.3$ Myr $\ll \tau_{disc}$. We therefore regard the cluster planetesimal number density uniform and reduced by $f_\star$. From equation (15), the number of captured

Table 1. Fraction of captured planetesimals lost due to ablation in field environments. Starred (*) entries are uncertain due to very low or none capture below the ablation limit.

Cluster	$R_p = 1$ m	$R_p = 10$ m	$R_p = 10^2$ m	$R_p = 10^3$ m
Ice	<1 per cent	37 per cent	31 per cent	32 per cent
Carbonate	<0.1 per cent	25 per cent	19 per cent	16 per cent
Rock	<0.1 per cent	16 per cent	10 per cent	6 per cent*
Iron	<0.1 per cent	9 per cent	<6 per cent	<1 per cent*
Field	$R_p = 1$ m	$R_p = 10$ m	$R_p = 10^2$ m	$R_p = 10^3$ m
Ice	7 per cent	78 per cent	66 per cent	57 per cent*
Carbonate	3.7 per cent	69 per cent	33 per cent	28 per cent*
Rock	1 per cent	53 per cent	16 per cent	28 per cent*
Iron	0.6 per cent	34 per cent	8 per cent	14 per cent*

large planetesimals is $N_{\rm captured}(>1\,{\rm km}) \sim 170 f_\star$ (and numerous smaller ones). If only a few large ∼1 km planetesimals are sufficient for seeding a given planetary system (Ormel & Kobayashi 2012; Levison, Kretke & Duncan 2015), or a larger number of smaller planetesimals (Booth et al. 2018), then only a small fraction of planetary systems is needed in order to seed all of the other protoplanetary systems in the cluster, $f_\star \approx 6 \times 10^{-3}$. Thus, even few stars that form planetesimals populate the entire cluster.

Similar arguments apply for the field, where reduction by $f_\star = 10^{-3}$ leads to capture of a few $R \sim 100$ m objects (since still $\tau_\star \sim 0.3\,{\rm Myr} \ll \tau_{\rm disc}$) during disc lifetime (and numerous smaller ones), which could also lead to subsequent planetesimal formation and field population. In addition, using the ∼50 times higher rates directly inferred from 'Oumuamua detection, even smaller fraction is required. We finally note that in the optimistic cases, even large planetary embryos of 10–30 km can be captured directly.

4.3 Binary star systems

The structure of the protoplanetary disc implicitly assumes a single star. However, most solar-type stars are in binary systems (Duchêne & Kraus 2013) and ∼20 per cent of exoplanets are in binary–star systems, some of them are in tight configurations (Thebault & Haghighipour 2015). The tidal interactions with the binary may disrupt or truncate the disc (Artymowicz & Lubow 1994). The lifetime of existing discs is also shortened (Müller & Kley 2012), $\tau_{\rm disc} \lesssim 1$ Myr, although a small fraction has discs even at $t \sim 10$ Myr (Kraus et al. 2012). Disc truncation will decrease the overall capture of small pebbles (in the geometric regime), while the capture of larger planetesimals will not be affected too much, since larger objects are captured at closer separations (see Fig. 4). Shorter disc lifetime equally and linearly decrease the total number of captured objects on all scales in the field. Cluster environment is less affected since the typical time-scale is the cluster crossing time, which is still shorter than the disc lifetime.

4.4 Planetesimal ablation

Planetesimal ablation could potentially affect, or even destroy a planetesimal as it crosses a PPD for the first time at high velocity. However, using simplified ablation models (Appendix B Pinhas, Madhusudhan & Clarke 2016) we find the expected ablation rates of the captured planetesimals in Table 1. ∼37 per cent of icy planetesimals and ∼16 per cent of rocky planetesimals of 10–10^3 m sizes are ablated during crossings in stellar clusters, and ∼78 per cent icy and ∼53 per cent rocky planetesimals of 10–10^3 m are ablated in field environments. Most of the ablated objects are in the range of 10–10^3 m; smaller pebbles are captured far enough, while larger bodies are harder to ablate. These do not significantly affect the overall results.

4.5 Chemical composition

The composition of meteorites in the Solar system is typically thought to relate to the primordial composition of the PPD. However, there is evidence for the existence of material captured from external sources. In particular, there is evidence for short-lived radioactive nuclei which were likely formed in a relatively nearby supernovae (Ouellette, Desch & Hester 2010). In addition, analysis of heavy ^{60}Fe –^{60} Ni isotopes in asteroids suggests the early injection of ^{60}Fe into the primordial PPD of our Sun (Bizzarro et al. 2007). The disc-capture mechanism allows for embedding such external material in the disc, and may help explain its origin.

These issues are not the main focus of our study, but it is interesting to consider the possibility of composition peculiarities in some meteorites originating from capture of material from other systems through this process. In particular, discovery of rocky/solid material older than the Solar system can provide a signature of material exchange.

4.6 Lithopanspermia

The exchange of rocky material between planetary systems may also be considered the leading mechanism for lithopanspermia; the transfer of living organisms or other biotic elements between different planetary systems (Napier 2004; Wesson 2010; Lingam & Loeb 2018). Biologically active material is expected to survive the ISM environment if the rock is above $m > 10$ g. Previously suggested dynamical exchange mechanisms are typically inefficient; most effective mechanisms requiring planetesimal encounter with a binary system, and subsequent capture, mostly through collisions with planets (Adams & Spergel 2005). Capture of planetary material following the dispersal of the host cluster is another suggested much more efficient mechanism (Levison et al. 2010; Perets & Kouwenhoven 2012); however, it introduces capture at typically large distances from the host star.

Even if a small fraction of biologically active material is ejected by interstellar planetesimals, the large efficiency of gas-assisted capture of 1 m-sized rocks could be far more efficient (as much as $\geq 10^5$ larger) than previously suggested lithopanspermia mechanisms (Adams & Spergel 2005).

5 SUMMARY

The current paradigm for planet formation involves a bottom up evolution of dust grains growing into planetesimals, then planetary embryos, and finally into planets in gaseous PPDs around young stars. One of the main open questions over the last 40 yr deals with the early stages of forming km-sized planetesimals from initially small dust grains (Weidenschilling 1977a; Chiang & Youdin 2010). Metre-sized pebbles experience a both significant gas drag and collisional erosion, and thus rapidly inspiral on to the star or fragment, respectively. Together, these issues give rise to the 'metre-sized barrier' problem in which the lifetime of small pebbles in the disc is too short compared with their growth rate. Thus, planet formation requires a 'jump' over small planetesimals as to

already begin with larger-sized planetesimals not susceptible to these growth constraints.

In this paper we have shown that the majority of planetary systems could have been 'seeded' by large ∼km-sized interstellar planetesimals. These could have formed elsewhere and then captured via gas drag experienced by the planetesimal as it passes through the PPD. This gives rise to early insertion of large planetesimals, and it thereby potentially alleviates the metre-sized barrier. The gas-assisted capture model does not account for the first generation of planetesimals, but rather makes their formation into a much easier exponentially small challenge. Planetesimal formation is no longer required to form in every planetary system in isolation, but rather in a small subset of systems, perhaps under fine tunes conditions. Even one successful planetesimal formation per system could populate the entire young stellar cluster with planetesimals, and perhaps even the young systems in the field.

We present a novel model of gas-assisted capture of interstellar planetesimals. We construct a robust, analytical model of the capture probability and overall capture rates as a function of the planetesimal size and orbit distribution, the protoplanetary disc structure, and the local environment. We verified the analytical derivation with direct Monte Carlo integrations and found good correspondence.

The gas-assisted capture model is compatible with late stage planetesimal growth models (snowball phase, pebble accretion, Xie et al. 2010; Lambrechts & Johansen 2012) and provides the missing link to the initial population of large dust grains and small planetesimals. In addition, the gas-assisted capture model supports the observation that asteroids formed big from a small number of asteroid families. The capture model can be tested by future measurements of composition peculiarities in some meteorites, which already has some evidence for early injection of heavy radioactive nuclei into the primordial protoplanetary disc of our Sun (Bizzarro et al. 2007; Ouellette et al. 2010).

Besides the importance for planet formation, the gas-assisted capture scenario allows for far more efficient exchange of biologically active material between different planetary systems. In fact, it could be as much as a million times more efficient than previously estimated (Adams & Spergel 2005), making the possibility for such panspermia events into the Solar system and/or between other planetary systems far more likely.

ACKNOWLEDGEMENTS

We thank Barak A. Katzir and Andrei P. Igoshev for stimulating discussions. EG acknowledges support by the Technion Irwin and Joan Jacobs Excellence Fellowship for outstanding graduate students. EG and HBP acknowledge support by Israel Science Foundation I-CORE grant 1829/12 and the Minerva center for life under extreme planetary conditions.

REFERENCES

Adachi I., Hayashi C., Nakazawa K., 1976, Prog. Theor. Phys., 56, 1756
Adams F. C., Spergel D. N., 2005, Astrobiology, 5, 497
Artymowicz P., Lubow S. H., 1994, ApJ, 421, 651
Belbruno E., Moro-Martín A., Malhotra R., Savransky D., 2012, Astrobiology, 12, 754
Bizzarro M., Ulfbeck D., Trinquier A., Thrane K., Connelly J. N., Meyer B. S., 2007, Science, 316, 1178
Blum J., 2018, Space Sci. Rev., 214, 52
Booth R. A., Meru F., Lee M. H., Clarke C. J., 2018, MNRAS, 475, 167
Chiang E. I., Goldreich P., 1997, ApJ, 490, 368
Chiang E., Youdin A. N., 2010, Ann. Rev. Earth Planet. Sci., 38, 493
Chiang E., Laughlin G., 2013, MNRAS, 431, 3444
Ćuk M., Burns J. A., 2004, Icarus, 167, 369
De Simone R., Wu X., Tremaine S., 2004, MNRAS, 350, 627
Dermott S. F., Christou A. A., Li D., Kehoe T. J. J., Robinson J. M., 2018, Nat. Astron., 2, 549
Do A., Tucker M. A., Tonry J., 2018, ApJ, 855, L10
Dohnanyi J. S., 1969, J. Geophys. Res., 74, 2531
Dones L., Gladman B., Melosh H. J., Tonks W. B., Levison H. F., Duncan M., 1999, Icarus, 142, 509
Duchêne G., Kraus A., 2013, ARA&A, 51, 269
Fujita T., Ohtsuki K., Tanigawa T., Suetsugu R., 2013, AJ, 146, 140
Grishin E., Perets H. B., 2015, ApJ, 811, 54
Grishin E., Perets H. B., 2016, ApJ, 820, 106
Hayashi C., 1981, Prog. Theor. Phys. Suppl., 70, 35
Hut P., Makino J., McMillan S., 1995, ApJ, 443, L93
Johansen A., Oishi J. S., Mac Low M.-M., Klahr H., Henning T., Youdin A., 2007, Nature, 448, 1022
Kraus A. L., Ireland M. J., Hillenbrand L. A., Martinache F., 2012, ApJ, 745, 19
Lambrechts M., Johansen A., 2012, A&A, 544, A32
Levison H. F., Duncan M. J., Brasser R., Kaufmann D. E., 2010, Science, 329, 187
Levison H. F., Kretke K. A., Duncan M. J., 2015, Nature, 524, 322
Lingam M., Loeb A., 2018, AJ, 156, 193
Meech K. J. et al., 2017, Nature, 552, 378
Melosh H. J., 2003, Astrobiology, 3, 207
Morbidelli A., 2018, Handbook of Exoplanets. Springer International, Cham
Morbidelli A., Bottke W. F., Nesvorný D., Levison H. F., 2009, Icarus, 204, 558
Müller T. W. A., Kley W., 2012, A&A, 539, A18
Napier W. M., 2004, MNRAS, 348, 46
Ormel C. W., Klahr H. H., 2010, A&A, 520, A43
Ormel C. W., Kobayashi H., 2012, ApJ, 747, 115
Ouellette N., Desch S. J., Hester J. J., 2010, ApJ, 711, 597
Perets H. B., Murray-Clay R. A., 2011, ApJ, 733, 56
Perets H. B., Kouwenhoven M. B. N., 2012, ApJ, 750, 83
Pinhas A., Madhusudhan N., Clarke C., 2016, MNRAS, 463, 4516
Raymond S. N., Cossou C., 2014, MNRAS, 440, L11
Raymond S. N., Armitage P. J., Veras D., Quintana E. V., Barclay T., 2018a, MNRAS, 476, 3031
Raymond S. N., Armitage P. J., Veras D., 2018b, ApJ, 856, L7
Simon J. B., Armitage P. J., Youdin A. N., Li R., 2017, ApJ, 847, L12
Thebault P., Haghighipour N., 2015, Planet Formation in Binaries, Springer-Verlag, Berlin, Heidelberg . p. 309
Valtonen M. et al., 2009, ApJ, 690, 210
Weidenschilling S. J., 1977a, Ap&SS, 51, 153
Weidenschilling S. J., 1977b, MNRAS, 180, 57
Wesson P. S., 2010, Space Sci. Rev., 156, 239
Windmark F., Birnstiel T., Güttler C., Blum J., Dullemond C. P., Henning T., 2012, A&A, 540, A73
Xie J.-W., Payne M. J., Thébault P., Zhou J.-L., Ge J., 2010, ApJ, 724, 1153
Youdin A. N., Goodman J., 2005, ApJ, 620, 459

APPENDIX A: DERIVATION OF THE GRAVITATIONAL FOCUSING REGIME

Here we derive equations (3.3.2) and (14). We start from a $\chi(4)$ distribution for the velocity:

$$\tilde{f}_V(v) = \frac{1}{2}\frac{v^3}{\sigma^4}\mathrm{e}^{-v^2/2\sigma^2} \tag{A1}$$

and uniform distribution of b^2, namely $f_B(b) \propto b$. In order to proceed, we define a new random variable $x \equiv (b/b_{\max})^{\alpha}(v_\infty/\sigma)^2$, $f_X(x)$, with α is related to the disc power-law density and defined in the main text.

First, we transform to $k = b^\alpha$ and $\mathrm{d}k = \alpha b^{\alpha-1}\mathrm{d}b$, so

$$f_K(k) = f_B(b)\frac{\mathrm{d}b}{\mathrm{d}k} = \frac{2k^{(2-\alpha)/\alpha}}{\alpha b_{\max}^2}. \tag{A2}$$

Similarly, the distribution function of $u \equiv v^2$ is

$$\tilde{f}_U(u) = \tilde{f}_V(v)\frac{\mathrm{d}v}{\mathrm{d}u} = \frac{1}{4}\frac{u}{\sigma^4}\mathrm{e}^{-u/2\sigma^2}. \tag{A3}$$

Now, the distribution of $z \equiv b^\alpha v^2$ is given by

$$\begin{aligned} f_Z(z) &= \iint \tilde{f}_U(t) f_K(k)\delta(ku - z)\mathrm{d}k\mathrm{d}u \\ &= \frac{1}{2\alpha\sigma^4 b_{\max}^2}\iint k^{(2-\alpha)/\alpha}\mathrm{e}^{-u/2\sigma^2}\delta(k - z/u)\mathrm{d}k\mathrm{d}u \\ &= \frac{z^{(2-\alpha)/\alpha}}{2\alpha\sigma^4 b_{\max}^2}\int_{z/k_{\max}}^{\infty} u^{(\alpha-2)/\alpha}\mathrm{e}^{-u/2\sigma^2}\mathrm{d}u, \end{aligned} \tag{A4}$$

where $\delta(s)$ is Dirac's delta distribution. Taking $x = z/b_{\max}^\alpha\sigma^2$ and $w = u/2\sigma^2$ we get

$$\begin{aligned} f_X(x) &= \frac{x^{(2-\alpha)/\alpha}}{\alpha}2^{1-2/\alpha}\int_{x/2}^{\infty} w^{1-2/\alpha}\mathrm{e}^{-w}\mathrm{d}w \\ &= 2^{-(2+\beta)/(1+\beta)}\frac{2+\beta}{1+\beta}\Gamma\left(\frac{\beta}{1+\beta}, \frac{x}{2}\right)x^{1/(1+\beta)} \end{aligned} \tag{A5}$$

where $\Gamma(s, z) = \int_z^\infty t^{s-1}e^{-t}\mathrm{d}t$ is the upper incomplete Gamma function. By using the integrals of the incomplete Gamma functions

$$\int x^{b-1}\Gamma(s, x)\mathrm{d}x = \frac{1}{b}\left(x^b\Gamma(s, x) - \Gamma(s + b, x)\right), \tag{A6}$$

the cumulative distribution function (CDF) is given by

$$F_X(x) = \int f_X(x)\mathrm{d}x = \left(\frac{x}{2}\right)^{\frac{2+\beta}{1+\beta}}\Gamma\left(\frac{\beta}{1+\beta}, \frac{x}{2}\right) - \Gamma\left(2, \frac{x}{2}\right). \tag{A7}$$

The linear expansion of the incomplete Gamma function is $\Gamma\left(s, \frac{x}{2}\right) = \Gamma(s) - \frac{x^s}{2^{-s}s} + \mathcal{O}\left(x^{s+1}\right)$, therefore the leading term in the CDF is

$$F_X(x) = 2^{-\frac{2+\beta}{1+\beta}}x^{\frac{2+\beta}{1+\beta}}\Gamma\left(\frac{\beta}{1+\beta}\right) - \frac{1+\beta}{\beta}2^{-\frac{2}{1+\beta}}x^2 - 1 + 2x^2. \tag{A8}$$

For $\beta > 0$, the first term is the dominant one, thus the capture probability is

$$f_c(R_p) = F_X(x) - F_X(0) = 2^{-\frac{2+\beta}{1+\beta}}x^{\frac{2+\beta}{1+\beta}}\Gamma\left(\frac{\beta}{1+\beta}\right) + \mathcal{O}\left(x^2\right). \tag{A9}$$

APPENDIX B: PLANETESIMAL ABLATION

The ablation equation is (Pinhas et al. 2016)

$$\frac{\mathrm{d}m}{\mathrm{d}t} = -\frac{C_H}{2}\frac{\rho_g v_{rel}^3 \pi R_p^2}{Q_{abl}}, \tag{B1}$$

where $m = 4\pi R_p^3\rho_p/3$ is the mass, ρ_p is the solid density, ρ_g is the gas density, C_H is the dimensionless heat transfer coefficient, v_{rel} is the relative velocity, R_p is the radius, and Q_{abl} is the specific ablation heat per unit mass. The ablation time is

$$t_{abl} = \left|\frac{R_p}{\mathrm{d}R_p/\mathrm{d}t}\right| \approx \frac{8}{C_H}\frac{\rho_p}{\rho_g}\frac{Q_{abl}}{v_{rel}^3}R_p \approx 10^4\left(\frac{R_p}{m}\right)\left(\frac{a}{\mathrm{au}}\right)^{53/14}\mathrm{s}. \tag{B2}$$

Significant ablation occurs if the ablation times is shorter than the minimum of the disc crossing time t_{cross} and the stopping time $t_{stop} = |mv_{rel}/F_D|$. For pebbles of $\gtrsim$1 m or larger bodies, the crossing time $t_{cross} = h/v_{rel}$ is the relevant. Comparing the time-scale gives the condition for ablation. The critical radial disc separation for ablation as a function of the planetesimal size and disc and planetesimal parameters is

$$a_{ab} = \sqrt{\frac{C_H}{8}\frac{\rho_g}{\rho_p}\frac{h}{R_p}\frac{v_{rel}^2}{Q_{abl}}}\,\mathrm{au}. \tag{B3}$$

For typical compositions of ices (see table 1 of Pinhas et al. 2016), $C_H = 0.01$, $Q_{abl} \approx 3 \times 10^{10}\,\mathrm{erg\ g^{-1}}$, $\rho_p = 1\,\mathrm{g\ cm^{-3}}$, and ρ_p and $v_{rel} \approx v_{esc}$ normalized to their values at 1 au the critical radial separation is

$$a_{ab} = \left(\frac{R}{7.3\,\mathrm{m}}\right)^{-1/2}\mathrm{au}. \tag{B4}$$

Fig. B1 shows the critical separation as a function of the planetesimal size for various compositions. We compare the critical separation for each composition with the cumulative fraction of captured planetesimal to estimate the fraction of ablated planetesimals. The results are summarized in Table 1.

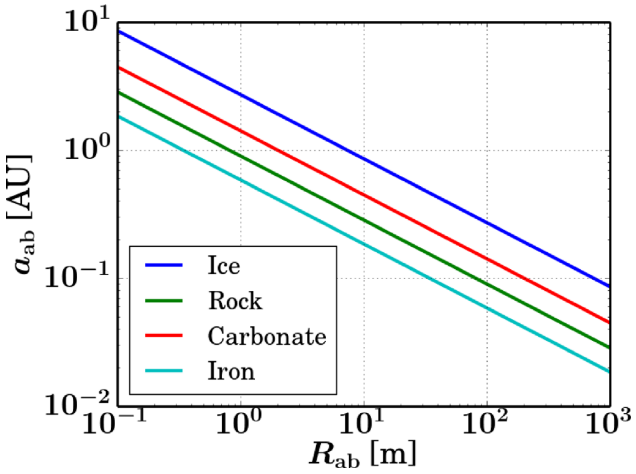

Figure B1. Critical separations for significant planetesimal ablation. Specific ablation heat coefficients and densities are taken from table 1 of Pinhas et al. (2016).

This paper has been typeset from a TEX/LATEX file prepared by the author.